

A Markov-based Framework for Handover Optimization in HetNets

Francesco Guidolin[†] Irene Pappalardo[†] Andrea Zanella[†] Michele Zorzi[†]

[†] Dept. of Information Engineering, University of Padova, via Gradenigo 6/B, 35131 Padova, Italy
{fguidolin, pappalar, zanella, zorzi}@dei.unipd.it

Abstract—The deployment of small cells in Heterogeneous Networks (HetNets) raises new challenges in relation to the Handover process and the mobility management. In fact, the performance of a mobile user within a HetNet scenario highly depends on the setting of the handover parameters in relation to other context parameters, such as the channel conditions and the user position and speed. In this paper, we derive a general theoretical analysis to characterize the user performance as a function of the mobility model, the power profile received from the neighboring cells, and the handover parameters. More in detail, we propose a Markov-based framework to model the user state during the handover process and, based on such model, we derive an optimal context-dependent handover criterion. The mathematical model is validated by means of simulations, showing that our strategy outperforms conventional handover optimization techniques by exploiting the context information.

Index Terms—Small cells, HetNets, Handover, discrete time Markov chain, context-awareness, mobile user.

I. INTRODUCTION

Global mobile data traffic is expected to increase nearly 11-fold between 2013 and 2018, reaching 15.9 exabytes per month by 2018 [1]. One of the most promising approaches to face this challenge is the so-called Heterogeneous Network (HetNet) paradigm, which basically consists in enriching the current cellular network with a number of smaller and simpler Base Stations (BSs), having widely varying transmit powers, coverage areas, carrier frequencies, backhaul connection types and communication protocols. The deployment of pico and/or femto BSs *within* the macro cell, indeed, can provide higher connection speed and better coverage to the mobile users located at the border of the macro cell or in regions with high traffic demand.

While increasing the efficiency of the cellular networks, HetNets also raise several technical challenges related to user management [2]. An important aspect is related to the management of user mobility that, differently from the classical cellular networks, has to deal with cells of widely varying coverage areas. In general, the handover (HO) process, standardized by the 3rd Generation Partnership Project (3GPP) [3], is triggered by the User Equipment (UE), which periodically measures the Reference Symbols Received Power (RSRP) from the surrounding cells. When the difference between the RSRP of a neighboring cell and the serving cell is higher than

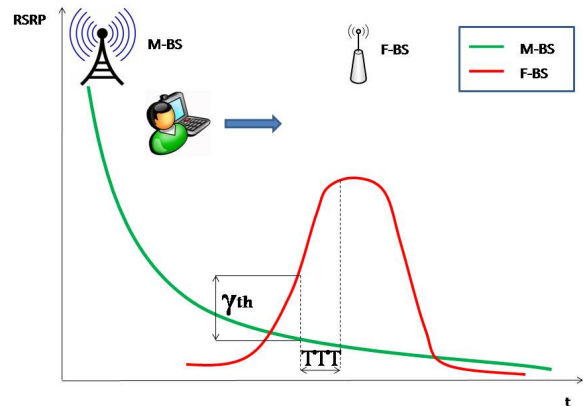


Fig. 1: Example of the decay of the power profile from the M-BS and F-BS as the UE moves away from the M-BS and towards the F-BS.

a fixed HO hysteresis value (event A3 in [4]), the HO process starts, as exemplified in Fig. 1. If this condition holds for a period of time equal to the *Time-To-Trigger* (TTT) parameter, the HO is finalized and the UE connects to the BS with the strongest RSRP.

The static setting of the HO hysteresis and TTT values adopted in traditional scenarios with only macro cells is no longer effective for HetNet systems, because of the large variety in cell characteristics [5]. With large values of TTT and hysteresis margin, the UE will likely experience a severe degradation of the RSRP during the TTT period when crossing a small cell, a problem that is generally referred to as *HO Failure*. On the other hand, short TTT and low hysteresis margin may cause *HO Ping-Pong*, i.e., frequent HOs to/from the M-BS, which yields performance losses due to signaling overhead and handover times. Reducing HO failure and ping-pong rates are clearly conflicting objectives, and the HO policy needs to trade off the two effects.

Several solutions in the literature consider to adapt some HO parameters to the UE mobility conditions. In [6] the authors evaluate the effect of the cell range expansion (CRE) on the HO failure and ping-pong rates, as a function of the UE mobility. In [7] and [8] the TTT parameter is adjusted according to the type of handover, e.g., macro-to-pico or pico-to-pico handover, and to the mobility state of the user. In [9] the authors propose an algorithm to set TTT and HO margin parameters by exploiting the concepts of dwell probability

and handover priority. The issue of the UE mobility change is presented in [10] and the hysteresis margin is adapted accordingly. In [11] an approximate expression of the HO performance has been derived without taking the fading effect into account.

Although these solutions improve the efficiency of HO in HetNets with respect to the static setting of the HO parameters, to the best of our knowledge a mathematical model that describes the HO performance as a function of the scenario parameters, such as the pathloss coefficients and the UE speed, is still lacking.

This paper attempts to make a step forward in this direction by first presenting a theoretical model that describes the evolution of the UE state along its trajectory, within a HetNet scenario. Second, we determine the expression of the average UE performance as a function of the HO parameters and other contextual parameters, such as the UE speed, the power profiles of the macro/pico/femto BSs, and the UE environment, e.g., urban or rural. We remark that the mathematical framework can accommodate different performance metrics, such as the HO failure rate, the ping-pong rate, or the average Shannon capacity, which is the one actually considered in this work. As a third contribution, we provide a context-aware HO policy (CAHP) that selects the HO parameters that maximize the performance metric with respect to UE environment and channel conditions. A similar work has been proposed in [12], where, however, the mathematical model is developed by considering the handover failure as the performance metric. Moreover, the authors in [12] make the assumption that the UE trajectory with respect to the position of the BSs is known to the UE. Our work, instead, proposes a more general model, and defines a context-aware HO strategy based on the more realistic assumption that the UE's trajectory with respect to the location of the BSs is unknown.

The rest of the paper is organized as follows. Sec. II introduces the channel propagation model and the HO mechanism, and derives the UE performance metric. Sec. III presents the analysis of the HO process by means of a discrete time Markov chain. Sec. IV formulates our context-aware HO optimization policy (CAHP) and depicts the results for different scenarios, in comparison also with other standard strategies. Finally, Sec. V concludes the paper.

II. SYSTEM MODEL

We focus on a basic scenario consisting of a macro BS (M-BS) and a femto BS (F-BS) placed at distance d_{MF} . For convenience, we define the UE's trajectory with respect to a reference circle \mathcal{H} of radius R centered at the F-BS. We assume that the UE moves at constant speed v , following a straight trajectory. With reference to the polar coordinate system depicted in Fig. 2, a trajectory is then uniquely identified by the angular coordinate ϕ of point \mathbf{b} where the UE crosses the border \mathcal{H} , and by the incidence angle ω formed by the trajectory with respect to the radius passing through \mathbf{b} . We assume that the UE can enter the femtocell from any point and with any angle, so that the parameters ϕ and ω are modeled as independent random variables with uniform distribution in the intervals $[0, 2\pi]$ and $[-\pi/2, \pi/2]$, respectively.

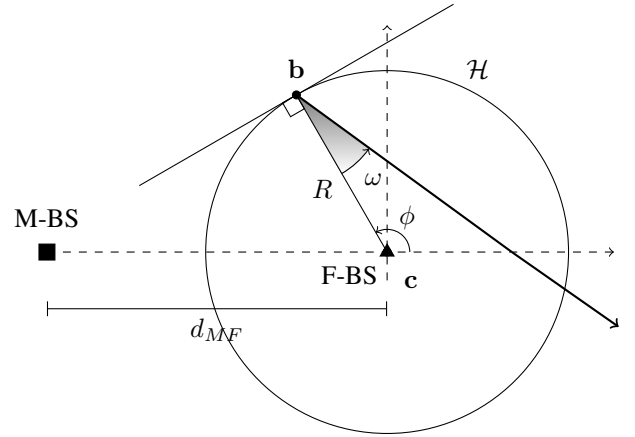


Fig. 2: Reference scenario: macrocell BS – M-BS (■), femtocell BS – F-BS (▲), and HO line \mathcal{H} approximated as a circle of radius R and center \mathbf{c} . Linear trajectory followed by a UE when entering the femtocell at point \mathbf{b} with incidence angle ω .

In the remainder of this section we describe the channel model, the HO process and the target performance metric considered in this work.

A. Propagation model

At time t , a mobile UE at position \mathbf{a} measures an RSRP $\Gamma_M(\mathbf{a}, t)$ from the M-BS, and $\Gamma_F(\mathbf{a}, t)$ from the F-BS.

We assume a path-loss plus fading propagation model [13], according to which the RSRP from the h -BS, with $h \in \{M, F\}$, is given by

$$\Gamma_h(\mathbf{a}, t) = \Gamma_h^{tx} g_h(\mathbf{a}) \alpha_h(t), \quad (1)$$

where Γ_h^{tx} is the transmit power of the h -BS, $g_h(\mathbf{a})$ is the pathloss gain, which depends only on the distance of point \mathbf{a} from the h -BS, while $\alpha_h(t)$ is the fast-fading channel gain at time t . We assume that the fading is Rayleigh distributed, i.e., $\alpha_h(t)$ is an exponential random variable with unit mean and coherence time

$$T_c = \sqrt{\frac{9}{16\pi}} \frac{1}{f_d} = \sqrt{\frac{9}{16\pi}} \frac{c}{vf_c}, \quad (2)$$

where f_d and f_c are the Doppler and the carrier frequency, respectively, c is the speed of light in vacuum and v is the UE speed. Due to fading, channel fluctuations can cause the HO process to be improperly triggered, thus increasing the ping-pong effect. The duration of the channel outage is a well studied metric in the literature to model this phenomenon [14].

Since the considered scenario is interference-limited, we can neglect the noise term, and approximate the Signal-to-Interference-and-Noise-Ratio (SINR) $\gamma_h(\mathbf{a}, t)$ experienced by an UE connected to h -BS at time t and in position \mathbf{a} as¹

$$\gamma_M(\mathbf{a}, t) = \frac{\Gamma_M(\mathbf{a}, t)}{\Gamma_F(\mathbf{a}, t)} \quad \text{if } h = M; \quad (3)$$

$$\gamma_F(\mathbf{a}, t) = \frac{\Gamma_F(\mathbf{a}, t)}{\Gamma_M(\mathbf{a}, t)} \quad \text{if } h = F. \quad (4)$$

¹The model can be extended to account for the interference from other cells, though for the sake of simplicity we neglect other interference sources.

It is convenient to decouple the deterministic and random components of the SINR by defining the processes

$$\xi_M(t) = \frac{\alpha_M(t)}{\alpha_F(t)}, \quad \xi_F(t) = \frac{\alpha_F(t)}{\alpha_M(t)}; \quad (5)$$

and

$$\bar{\gamma}_M(\mathbf{a}) = \frac{\Gamma_M^{tx} g_M(\mathbf{a})}{\Gamma_F^{tx} g_F(\mathbf{a})}, \quad \bar{\gamma}_F(\mathbf{a}) = \frac{\Gamma_F^{tx} g_F(\mathbf{a})}{\Gamma_M^{tx} g_M(\mathbf{a})}; \quad (6)$$

so that

$$\gamma_h(\mathbf{a}, t) = \bar{\gamma}_h(\mathbf{a})\xi_h(t), \quad h \in \{M, F\}.$$

B. Handover performance model

The HO process is driven by the UE's instantaneous SINR. If the SINR drops below the HO threshold γ_{th} , the TTT timer is initialized to a certain value T and the countdown starts. Whenever the SINR returns above the HO threshold, however, the countdown is aborted and the HO procedure is interrupted. Conversely, if the SINR remains below the threshold for the entire interval T , then the UE disconnects from the serving BS and connects to the new BS. This switching process takes a time T_H that accounts for the network procedures to connect the UE to the target BS. For any given point \mathbf{a} , we can then define the connection state S of the UE to be M , F or H depending on whether the UE is connected to the **M**-BS, the **F**-BS or is temporarily disconnected because **H**anding over from one to the other.

Given an arbitrary straight path ℓ , we define the mean trajectory performance as

$$C_\ell = \frac{1}{|\ell|} \int_\ell \sum_{S \in \{M, F, H\}} C_S(\mathbf{a}) \chi_{\mathbf{a}}(S) d\mathbf{a}; \quad (7)$$

where $|\ell|$ is the trajectory's length, \int_ℓ is a line integral, $\chi_{\mathbf{a}}(S)$ is 1 if the UE's state at point \mathbf{a} is S and zero otherwise, while $C_S(\mathbf{a})$ is the performance experienced by the UE at point \mathbf{a} along the trajectory, when it is in state $S \in \{M, F, H\}$.

Since the UE can follow any trajectory, we average the capacity along all the straight lines of length L that enter the femtocell with random incidence angle, thus obtaining²

$$C_L = \frac{1}{L\pi} \int_{-\pi/2}^{\pi/2} \int_0^L \sum_{S \in \{M, F, H\}} C_S(\mathbf{a}(x, \omega)) \chi_{\mathbf{a}(x, \omega)}(S) dx d\omega, \quad (8)$$

with $\mathbf{a}(x, \omega)$ being the point at distance x from \mathbf{b} along the trajectory with incidence angle ω .

Now, the term $\chi_{\mathbf{a}(x, \omega)}(S)$ is random, depending on the evolution of the SINR in the previous time interval of length T . Taking the expectation of (8) with respect to the random variables $\xi(t)$ defined in (5), we hence get

$$\bar{C}_L = \frac{1}{L\pi} \int_{-\pi/2}^{\pi/2} \int_0^L \sum_{S \in \{M, F, H\}} \bar{C}_S(\mathbf{a}(x, \omega)) P_S[\mathbf{a}(x, \omega)] dx d\omega, \quad (9)$$

²For the symmetry of the problem, the entrance point \mathbf{b} is irrelevant. Moreover L is chosen to be large enough to allow the UE to be eventually connected to the **M**-BS.

where $\bar{C}_S(\mathbf{a}(x, \omega))$ is the average performance at point $\mathbf{a}(x, \omega)$, given that the UE's state at point $\mathbf{a}(x, \omega)$ is S , whose probability is

$$P_S[\mathbf{a}(x, \omega)] = \mathbb{E} [\chi_{\mathbf{a}(x, \omega)}(S)]. \quad (10)$$

In this paper, we take the average Shannon capacity experienced by the UE while crossing the femtocell as the performance metric. Hence, for $S \in \{M, F\}$ we define

$$\begin{aligned} \bar{C}_S(\mathbf{a}) &= \mathbb{E} [\log_2(1 + \gamma_S(\mathbf{a}, t))] \\ &= \log_2(\bar{\gamma}_S(\mathbf{a})) \frac{\bar{\gamma}_S(\mathbf{a})}{\bar{\gamma}_S(\mathbf{a}) - 1}; \end{aligned} \quad (11)$$

where the expression in the last row is derived in the Appendix. In order to account for the various costs of the handover process (energy, time, signaling, etc), we assume zero capacity when the UE is switching from one BS to the other, i.e.,

$$C_H(\mathbf{a}) = 0.$$

Unfortunately, the fading process is time-correlated, which makes the computation of (10) very complex. To overcome this problem, in place of the continuous time model we consider a discrete time model where the UE's trajectory is observed at time epochs spaced apart by the fading coherence time T_c . In this way, at each sample time we can approximately assume an independent fading value. Note that the sampling time varies with the UE's speed, see (2). Nonetheless, the distance covered by the UE in a time slot is fixed and equal to

$$\Delta_c = vT_c = \sqrt{\frac{9}{16\pi}} \frac{c}{f_c}. \quad (12)$$

We can then define the *average capacity* \bar{C}_L with respect to this sampled space as

$$\bar{C}_L = \frac{1}{\pi} \int_{-\pi/2}^{\pi/2} \frac{1}{N_L} \sum_{k=1}^{N_L} \sum_{S \in \{M, F, H\}} \bar{C}_S(\mathbf{a}_k(\omega)) P_S[\mathbf{a}_k(\omega)] d\omega \quad (13)$$

where

$$N_L = \left\lceil \frac{L}{\Delta_c} \right\rceil \quad (14)$$

is the total number of sample points along the trajectory, and $P_S[\mathbf{a}_k(\omega)]$ is the probability that at sample point \mathbf{a}_k along its trajectory the UE is in state $S \in \{M, F, H\}$. In the next section, we describe a Markov model to compute the probabilities $P_S[\mathbf{a}_k(\omega)]$. In Sec. IV, we then propose our context-aware Handover policy (CAHP) that dynamically selects the T value that maximizes (13) for different UE speed and environment parameters.

III. MARKOV ANALYSIS OF THE HO PERFORMANCE

In this section we model the HO process by means of a non homogeneous discrete time Markov Chain (MC). To begin with, we denote by N_T and N_H the number of space slots covered by the UE in time T and T_H , respectively, i.e.,

$$N_T = \left\lceil \frac{vT}{\Delta_c} \right\rceil, \quad N_H = \left\lceil \frac{vT_H}{\Delta_c} \right\rceil. \quad (15)$$

At every step, the UE moves along its trajectory, and the SINR changes accordingly. As explained in the previous section,

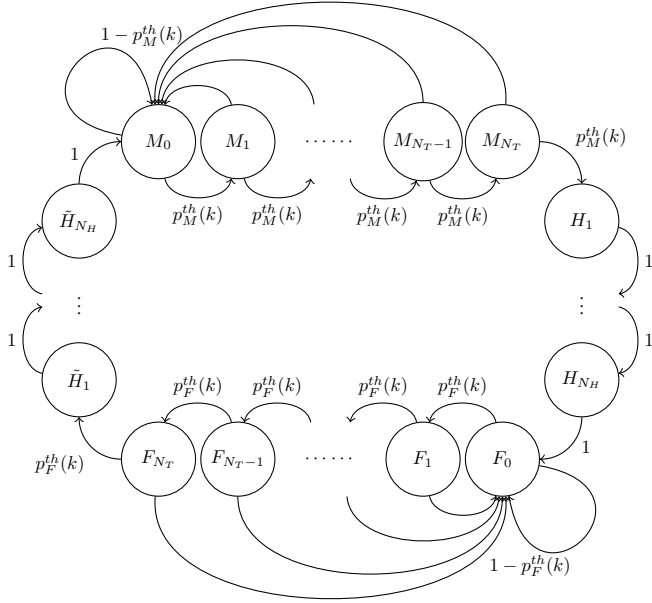


Fig. 3: Non homogeneous discrete time Markov chain referred to a scenario with arbitrary N_T and N_H . The transition probabilities are given by (17) and (18).

the HO process is started whenever the SINR drops below a certain threshold γ_{th} . We then define M_j and F_j , with $j \in \{0, \dots, N_T\}$, as the MC state that is entered when the UE is connected to the M-BS or F-BS, respectively, and the SINR has remained below γ_{th} for j consecutive steps. Furthermore, we define H_j and \tilde{H}_j , $j \in \{1, \dots, N_H\}$, as the MC states entered when the UE performs the macro-to-femto and femto-to-macro handover, respectively.

Assume that, at step k , the MC is in state M_j . In the following step, the MC evolves from M_j to M_{j+1} if $\gamma_M(\mathbf{a}_k, kT_c) < \gamma_{th}$, otherwise the MC returns to M_0 since the TTT counter is reset. Conversely, if the SINR remains below threshold when the MC is in state M_{N_T} , the UE starts the HO process to the F-BS and the MC enters state H_1 . In the following N_H steps the MC deterministically crosses all the handover states H_j and ends up in state F_0 , regardless of the channel conditions. At this point, the UE is connected to F-BS, and the evolution of the MC is conceptually identical to that seen for the M_j states.

A graphical representation of the non homogeneous discrete time MC is shown in Figure 3, with the transition probabilities that will be explained below.

A. Transition probabilities and transition matrix

The cumulative distribution function $F_\xi(x)$ of the random variable ξ , defined as the ratio of two exponential random variables with equal mean, is given by

$$F_\xi(x) = P[\xi \leq x] = \frac{x}{x+1}, \quad x \in [0, +\infty]. \quad (16)$$

Using (16), the transition probability from state M_j to M_{j+1} , with $j \in \{0, \dots, N_T\}$, at step k , is given by

$$p_M^{th}(k) = P[\gamma_M(\mathbf{a}_k, kT_c) < \gamma_{th}] = \frac{\gamma_{th}}{\gamma_{th} + \bar{\gamma}_M(\mathbf{a}_k)}. \quad (17)$$

Similarly, the transition probability from F_j to F_{j+1} is given by

$$p_F^{th}(k) = P[\gamma_F(\mathbf{a}_k, kT_c) < \gamma_{th}] = \frac{\gamma_{th}}{\gamma_{th} + \bar{\gamma}_F(\mathbf{a}_k)}. \quad (18)$$

Note that (17) and (18) vary along the UE trajectory because of the pathloss, so that the MC is indeed non-homogeneous.

Without loss of generality, we can arrange the states according to the order $\{M_j\}$, $\{H_j\}$, $\{F_j\}$, and $\{\tilde{H}_j\}$, and follow the increasing order of the index j within the same set of states. The system transition matrix $\mathbf{P}(k)$ at the k -th step can then be expressed with the following sub block structure

$$\mathbf{P}(k) = \begin{bmatrix} \mathbf{M}(k) & \mathbf{V}_M^H(k) & \emptyset & \emptyset \\ \emptyset & \mathbf{H}(k) & \mathbf{V}_H^F(k) & \emptyset \\ \emptyset & \emptyset & \mathbf{F}(k) & \mathbf{V}_F^{\tilde{H}}(k) \\ \mathbf{V}_H^M(k) & \emptyset & \emptyset & \tilde{\mathbf{H}}(k) \end{bmatrix} \quad (19)$$

where the submatrices $\mathbf{M}(k)$, $\mathbf{F}(k)$, $\mathbf{H}(k)$, and $\tilde{\mathbf{H}}(k)$ are the square transition matrices within the sets $\{M_j\}$, $\{F_j\}$, $\{H_j\}$, and $\{\tilde{H}_j\}$, respectively, while $\mathbf{V}_X^Y(k)$ are the rectangular transition matrices from the set X to the set Y . All the other blocks are null and represented by the symbol \emptyset . From the previous analysis, $\mathbf{M}(k)$ is given by

$$\mathbf{M}(k) = \begin{bmatrix} 1 - p_M^{th}(k) & p_M^{th}(k) & 0 & \dots & 0 \\ 1 - p_M^{th}(k) & 0 & p_M^{th}(k) & \dots & 0 \\ \vdots & \vdots & \vdots & \ddots & 0 \\ 1 - p_M^{th}(k) & 0 & 0 & \dots & p_M^{th}(k) \\ 1 - p_M^{th}(k) & 0 & 0 & \dots & 0 \end{bmatrix}. \quad (20)$$

$\mathbf{F}(k)$ is the same as $\mathbf{M}(k)$ with $p_F^{th}(k)$ in place of $p_M^{th}(k)$, while

$$\mathbf{H}(k) = \tilde{\mathbf{H}}(k) = \begin{bmatrix} 0 & 1 & 0 & \dots & 0 \\ 0 & 0 & 1 & \dots & 0 \\ \vdots & \vdots & \vdots & \ddots & 0 \\ 0 & 0 & \dots & \dots & 1 \\ 0 & 0 & \dots & \dots & 0 \end{bmatrix}. \quad (21)$$

Finally,

$$\mathbf{V}_H^F(k) = \mathbf{V}_H^M(k) = \begin{bmatrix} \emptyset & \emptyset \\ 1 & \emptyset \end{bmatrix}, \quad (22)$$

and

$$\mathbf{V}_M^H(k) = \begin{bmatrix} \emptyset & \emptyset \\ p_M^{th}(k) & \emptyset \end{bmatrix}, \quad \mathbf{V}_F^{\tilde{H}}(k) = \begin{bmatrix} \emptyset & \emptyset \\ p_F^{th}(k) & \emptyset \end{bmatrix}. \quad (23)$$

Once the transition matrix is defined, the state probability vector $\mathbf{p}(k)$ at the k -th step is given by

$$\mathbf{p}(k) = \mathbf{p}(0) \prod_{i=0}^{k-1} \mathbf{P}(i) \quad (24)$$

where $\mathbf{p}(0)$ is the state probability vector at the starting point of the UE trajectory. Assuming that the UE starts its path very close to the M-BS, we set the initial probabilities to 1 for M_0 and 0 for all the other states, so that

$$\mathbf{p}(0) = [1 \ 0 \ \dots \ 0]. \quad (25)$$

We can then compute the probability that the UE is in state $S \in \{M, F, H\}$ at any given point \mathbf{a}_k , $k \in \{1, \dots, N_L\}$, as

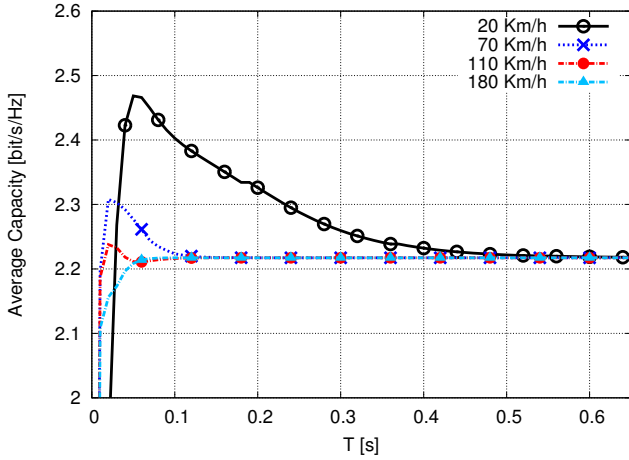


Fig. 4: Analytical average capacity obtained for different speeds, as a function of T .

the sum of the probabilities of the states $\{M_j\}$, $\{F_j\}$, and $\{H_j\} \cup \{\tilde{H}_j\}$, respectively, at step k , i.e.,

$$P_S[\mathbf{a}_k] = \sum_{i \in \{S_j\}} p_i(k), \quad (26)$$

where $p_i(k)$ is the i -th entry of the state probability vector (24).

IV. PERFORMANCE EVALUATION

In this section we analyze the results obtained from the mathematical model developed in Sec. II and Sec. III, and we compare the simulated performance of our context-aware handover policy (CAHP) that maximizes the metric (13), against the standard handover process using static TTT values (FIX). We assume a scenario composed by a M-BS with transmission power of 46 dBm and a F-BS with transmission power of 24 dBm [15]. The BSs are placed 500 m apart. Furthermore, we set $T_H = 200$ ms, while T is varied with a granularity of 10 ms.

Fig. 4 shows the analytical average capacity \bar{C}_L given by (13) for different speeds, as a function of T . We note that the curves show a similar trend for all speed values. The sharp capacity drop for low T values is due to the ping-pong effect, which is indeed alleviated when using longer T values. In particular, the longer the channel coherence time (i.e., the lower the speed v), the larger the T required to avoid the ping pong effect. For high T values, all curves reach an asymptotic value that corresponds to the average capacity achievable when handover is not performed. The optimal T is then given by a tradeoff between avoiding ping-pong effects and performing handover rapidly, within the femto cell coverage area. Note that, for very high speeds, the maximum capacity corresponds to the asymptotic capacity. In this case, the optimal handover policy simply consists in avoiding the handover, since the performance loss due to HO process is not compensated by the capacity gain obtained by connecting to the F-BS.

Fig. 5 shows the optimal T values obtained for different speeds and scenarios. In practice, we vary the pathloss coefficients from the macro and femto BSs to change the RSRP profile and the femto cell coverage area: we obtain a small

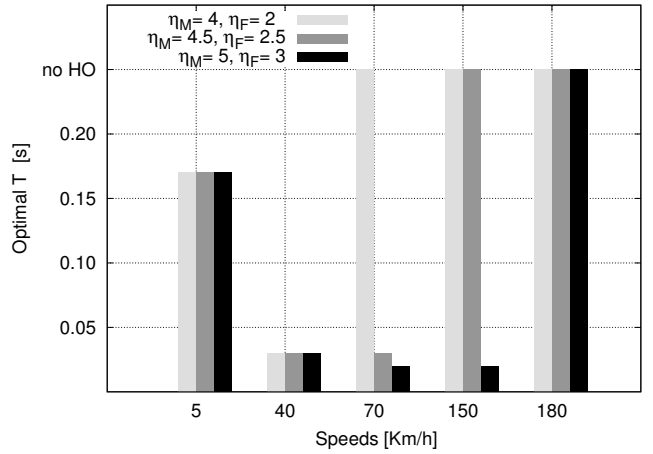


Fig. 5: Optimal T values obtained for different speeds and scenarios according to CAHP approach.

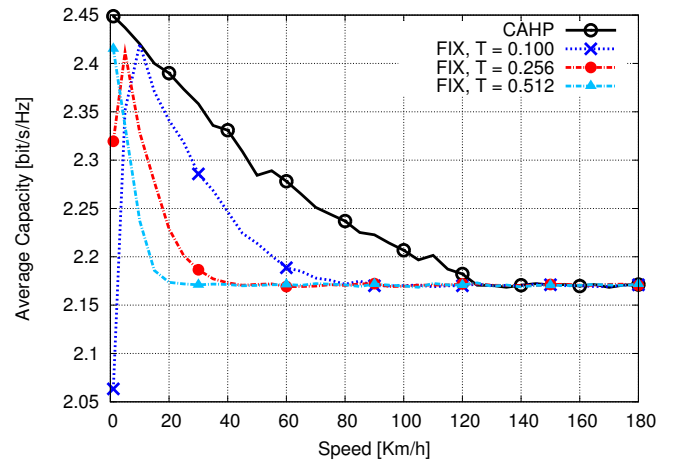


Fig. 6: Average capacity obtained with different approaches, as a function of the UE speed.

cell coverage area for $\eta_F = 2, \eta_M = 4$, a medium coverage for $\eta_F = 2.5, \eta_M = 4.5$, and a large one for $\eta_F = 3, \eta_M = 5$. We note that skipping handover is optimal for speeds larger than a threshold that is proportional to the femto cell range. In particular, for large cells, the losses due the handover are balanced by the higher capacity obtained by connecting to the F-BS. For a speed below threshold, instead, the optimal T value is the minimum value that avoids ping-pong events due to fast fading and, hence, only depends on the coherence time, which is independent of the pathloss coefficients of the different cells.

In the following we evaluate the performance achieved by the CAHP approach through Montecarlo simulations. In particular, we compare the mean capacity obtained by CAHP against the capacity of FIX policies that use constant TTT values, with $T \in \{0.100 \text{ s}, 0.256 \text{ s}, 0.512 \text{ s}\}$, irrespective of the UE speed, and of the other channel parameters. In the simulation we consider path loss coefficients $\eta_F = 2.5$ and $\eta_M = 4.5$ for F-BS and M-BS, respectively, and the fast fading model presented in Sec. II.

Fig. 6 shows the average capacity obtained in the simulations. At low speeds, the performance of the FIX policy

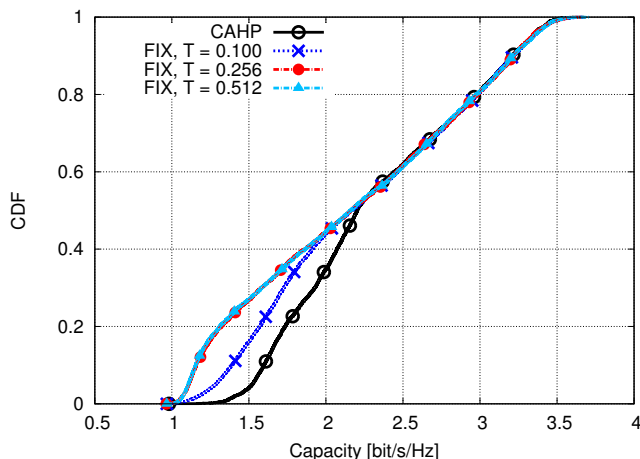


Fig. 7: Average capacity CDF for different approaches.

suffers from the ping-pong effect due to low T values, while CAHP adopts a larger T that avoids HO triggering due to fast-fading fluctuations. Conversely, for higher speeds, CAHP outperforms the FIX policy by adopting sufficiently low T values to avoid the ping-pong effects, while not excessively delaying the switching to the F-BS. We note that, at high speeds, all curves saturate to the same value corresponding, as in the analytical model, to the average capacity achieved when the UE remains always connected to the M-BS. In particular, the higher the fixed T value, the lower the speed beyond which HO is never performed, and the higher the capacity loss in comparison with CAHP that, instead, performs handover. Once again, we observe that, for high speeds, the optimal HO policy consists in not performing the handover to the F-BS, to avoid the loss due to the two T_H in a short time interval. In this case, all the policies with sufficiently large T obtain the same results. Note that the saturation capacity given by simulations slightly differs from that given by the Markov model, as reported in Fig. 4. This small discrepancy is likely due to the simplifying assumption of the analytical model, which considers a perfectly homogeneous scenario around the femtocell center c . The simulations, instead, consider the actual location of both BSs and the actual power received at any given point by each of them.

Finally, Fig. 7 shows the cumulative distributive function (CDF) of the average capacity for a user speed of $v = 40$ Km/h. We note that the improvement provided by CAHP is concentrated in the lower part of the CDF. These values correspond to the trajectories that cross the femtocell coverage area close to the F-BS. In particular, in this region, a small T makes it possible to exploit the signal from F-BS and to gain up to 50% in capacity in comparison with the case with larger T . On the contrary, the higher part of the CDF corresponds to trajectories far from the F-BS; in this case the average capacity is basically unaffected by T since handover is skipped in most cases.

V. CONCLUSIONS AND FUTURE WORK

In this work we proposed a novel context aware policy to optimize the handover procedure in HetNets. We computed the user average capacity exploiting a novel analytical framework

based on a Markov chain that considers the evolution of the UE state during the handover process. Then, we derived the handover strategy that maximizes the UE average capacity in different scenarios. Finally, we showed that the performance obtained with the proposed policy outperforms a standard TTT fixed policy.

The results emphasize the importance of a context-aware handover optimization in next generation cellular networks.

As future work we plan to extend the scenario to a more complex network and enlarge the optimization framework considering BS loads and the QoS user requirements. We plan also to couple the model with a machine-learning context estimator.

APPENDIX

From (16), the probability density function of ξ is given by

$$f_{\xi}(x) = \frac{d}{dx} F_{\xi}(x) = \frac{1}{(x+1)^2}, \quad x \in [0, +\infty]. \quad (27)$$

Given $\bar{\gamma}$, the expectation of $\log_2(1 + \bar{\gamma}\xi)$ is computed as

$$\begin{aligned} & \int_0^{+\infty} \log_2(1 + \bar{\gamma}x) f_{\xi}(x) dx \\ &= \int_0^{+\infty} \log_2(1 + \bar{\gamma}x) \frac{1}{(x+1)^2} dx \\ &= \frac{\bar{\gamma}}{\bar{\gamma}-1} \log_2 \left(\frac{1 + \bar{\gamma}x}{1+x} \right) \Big|_0^{+\infty} \\ &= \frac{\bar{\gamma}}{\bar{\gamma}-1} \log_2(\bar{\gamma}) \end{aligned}$$

where integration by parts was used to solve the integral.

REFERENCES

- [1] Cisco, Cisco Visual Networking Index: Global Mobile Data Traffic Forecast Update, 20132018, Feb. 2014, *White Paper*, pp. 1–40.
- [2] J. G. Andrews, "Seven ways that HetNets are a cellular paradigm shift," *IEEE Comm. Magazine*, vol. 51, no. 3, pp. 136–144, March 2013.
- [3] 3GPP TR 36.839, "Evolved Universal Terrestrial Radio Access (E-UTRA); Mobility enhancements in heterogeneous networks (Release 11)", version 11.0.0, September 2012.
- [4] 3GPP TS 36.331, "Protocol Specification; Radio Resource Control," v.10.4.0, Dec. 2011.
- [5] D. López-Pérez, I. Guvenc, X. Chu, "Mobility management challenges in 3GPP heterogeneous networks," *IEEE Comm. Magazine*, vol. 50, no. 12, pp. 70–78, December 2012.
- [6] K. Kitagawa, T. Komine, T. Yamamoto, S. Konishi, "Performance evaluation of handover in LTE-Advanced systems with pico cell Range Expansion," *IEEE PIMRC 2012*, pp. 1071–1076, 9–12 Sept. 2012.
- [7] S. Barbera, P. H. Michaelsen, M. Saily, K. Pedersen, "Improved mobility performance in LTE co-channel HetNets through speed differentiated enhancements," *IEEE Globecom*, pp. 426–430, 3–7 Dec. 2012.
- [8] M. Peng, D. Liang, Y. Wei, J. Li, H. Chen, "Self-configuration and self-optimization in LTE-advanced heterogeneous networks," *IEEE Comm. Magazine*, vol. 51, no. 5, pp. 36–45, May 2013.
- [9] C. Ma, G. Yu, J. Zhang, "Inter-Tier Handover in Macrocell/Relay/Femtocell Heterogeneous Networks," *IEEE VTC Spring 2012*, pp. 1–5, 6–9 May 2012.
- [10] K. Kitagawa, T. Komine, T. Yamamoto, S. Konishi, "A handover optimization algorithm with mobility robustness for LTE systems," *IEEE PIMRC 2011* pp. 1647–1651, 11–14 Sept. 2011.
- [11] F. Guidolin, I. Pappalardo, A. Zanella, M. Zorzi, "Context-Aware Handover in HetNets," *European Conference on Networks and Communications (EuCNC)*, 2326 June 2014, Bologna, Italy.
- [12] Q. Liao, F. Penna, S. Stanczak, R. Zhe, P. Fertl, "Context-aware handover optimization for relay-aided vehicular terminals," *IEEE 14th Workshop on Signal Processing Advances in Wireless Communications*, pp. 555–559, 16–19 June 2013.

- [13] A. Goldsmith, *Wireless Communications*. Cambridge University Press, New York, NJ, 2005.
- [14] M. Zorzi, "Outage and error events in bursty channels," *IEEE Transactions on Communications*, vol. 46, no. 3, pp. 349356, March 1998.
- [15] R. Tanbourgi, S. Singh, J. G. Andrews, F. K. Jondral, Friedrich K., "Analysis of Non-Coherent Joint-Transmission Cooperation in Heterogeneous Cellular Networks;" to appear in *IEEE ICC 2014*.